

Volume 3 • Issue 2 • November / December 2012

Editor-in-Chief
Professor Rajab Chaloo

INTERNATIONAL JOURNAL OF
APPLIED SCIENCES (IJAS)

ISSN : 2180-1258

Publication Frequency: 6 Issues / Year

CSC PUBLISHERS
<http://www.cscjournals.org>

Copyrights © 2012 Computer Science Journals. All rights reserved.

INTERNATIONAL JOURNAL OF APPLIED SCIENCES (IJAS)

VOLUME 3, ISSUE 2, 2012

**EDITED BY
DR. NABEEL TAHIR**

ISSN (Online): 2180-1258

International Journal of Applied Sciences is published both in traditional paper form and in Internet. This journal is published at the website <http://www.cscjournals.org>, maintained by Computer Science Journals (CSC Journals), Malaysia.

IJAS Journal is a part of CSC Publishers

Computer Science Journals

<http://www.cscjournals.org>

INTERNATIONAL JOURNAL OF APPLIED SCIENCES (IJAS)

Book: Volume 3, Issue 2, November / December 2012

Publishing Date: 31-12-2012

ISSN (Online): 2180-1258

This work is subjected to copyright. All rights are reserved whether the whole or part of the material is concerned, specifically the rights of translation, reprinting, re-use of illustrations, recitation, broadcasting, reproduction on microfilms or in any other way, and storage in data banks. Duplication of this publication of parts thereof is permitted only under the provision of the copyright law 1965, in its current version, and permission of use must always be obtained from CSC Publishers.

IJAS Journal is a part of CSC Publishers

<http://www.cscjournals.org>

© IJAS Journal

Published in Malaysia

Typesetting: Camera-ready by author, data conversion by CSC Publishing Services – CSC Journals, Malaysia

CSC Publishers, 2012

EDITORIAL PREFACE

This is *Second Issue* of Volume *Three* of the International Journal of Applied Sciences (IJAS). IJAS is an International refereed journal for publication of current research in applied sciences. IJAS publishes research papers dealing primarily with the research aspects of Applied Sciences in general. Publications of IJAS are beneficial for researchers, academics, scholars, advanced students, practitioners, and those seeking an update on current experience, state of the art research theories and future prospects in relation to applied science. Some important topics covers by IJAS are agriculture, architectural, audio, automotive, military ammunition, military technology, military etc.

The initial efforts helped to shape the editorial policy and to sharpen the focus of the journal. Starting with Volume 4, 2013, IJAS will be appearing with more focused issues. Besides normal publications, IJAS intend to organized special issues on more focused topics. Each special issue will have a designated editor (editors) – either member of the editorial board or another recognized specialist in the respective field.

This journal publishes new dissertations and state of the art research to target its readership that not only includes researchers, industrialists and scientist but also advanced students and practitioners. IJAS seeks to promote and disseminate knowledge in the applied sciences, natural and social sciences industrial research materials science and technology, energy technology and society including impacts on the environment, climate, security, and economy, environmental sciences, physics of the games, creativity and new product development, professional ethics, hydrology and water resources, wind energy.

IJAS editors understand that how much it is important for authors and researchers to have their work published with a minimum delay after submission of their papers. They also strongly believe that the direct communication between the editors and authors are important for the welfare, quality and wellbeing of the Journal and its readers. Therefore, all activities from paper submission to paper publication are controlled through electronic systems that include electronic submission, editorial panel and review system that ensures rapid decision with least delays in the publication processes.

To build its international reputation, we are disseminating the publication information through Google Books, Google Scholar, Directory of Open Access Journals (DOAJ), Open J Gate, ScientificCommons, Docstoc, Scribd, CiteSeerX and many more. Our International Editors are working on establishing ISI listing and a good impact factor for IJAS. We would like to remind you that the success of our journal depends directly on the number of quality articles submitted for review. Accordingly, we would like to request your participation by submitting quality manuscripts for review and encouraging your colleagues to submit quality manuscripts for review. One of the great benefits we can provide to our prospective authors is the mentoring nature of our review process. IJAS provides authors with high quality, helpful reviews that are shaped to assist authors in improving their manuscripts.

Editorial Board Members

International Journal of Applied Sciences (IJAS)

EDITORIAL BOARD

EDITOR-in-CHIEF (EiC)

Professor. Rajab Chaloo
Texas A&M University
United States of America

ASSOCIATE EDITORS (AEiCs)

Dr. Nikolaos Kourkoumelis

University of Ioannina
Greece

Professor seifedine kadry

American University of the Middle East
Kuwait

EDITORIAL BOARD MEMBERS (EBMs)

Dr. Sullip Kumar Majhi

Indian Council of Agricultural Research
India

Dr. Srung Smanmoo

National Center for Genetic Engineering and Biotechnology
Thailand

Professor Naji Qatanani

An-Najah National University
Palestine

Dr. Shuhui Li

The University of Alabama
United States of America

Professor Vidosav D. Majstorovich

University of Belgrade
Serbia

Dr Raphael Muzondiwa Jingura

Chinhoyi University of Technology
Zimbabwe

Professor Jian John Lu

University of South Florida
USA

Dr Tadjine Hadj Hamma

IAV GmbH, Technical University Clausthal
Germany

Dr Raphael Muzondiwa Jingura
Chinhoyi University of Technology - Zimbabwe
Zimbabwe

Assistant Professor Chibli Joumaa
American University of the Middle East
Kuwait

Assistant Professor Dr. Adel Eldenglawey
South Valley University
Egypt

Assistant Professor M. Shahria Alam
The University of British Columbia
Canada

TABLE OF CONTENTS

Volume 3, Issue 2, November / December 2012

Pages

- 21 - 34 Experimental Investigation of Flame Kernel in Turbulent Partial Premixed Flames
A. M. Elbaz, Mohy Mansour, Diaaeldin Mohamed
- 35 - 46 A Thresholding Method to Estimate Quantities of Each Class
Kenta Azuma, Kohei Arai, Ishitsuka Naoki

Experimental Investigation of Flame Kernel in Turbulent Partial Premixed Flames

A. M. Elbaz

*Faculty of Engineering/Mechanical Power Engineering Department
Helwan University
Cairo, 11718, Egypt*

ayman_alhagrasy@m-eng.helwan.edu.eg

Mohy Mansour

*Faculty of Engineering/Mechanical Power Engineering Department,
Cairo University, Egypt*

mansour@niles.edu.eg

Diaaeldin Mohamed

*Faculty of Engineering/Mechanical Power Engineering Department,
Cairo, University, Egypt*

diaa.eldin@aucegypt.edu

Abstract

The flame kernel propagation is believed to be influenced by many operating parameters such as mixing level, turbulent intensity, and the mixture equivalence ratio. The purpose of this study is to investigate the effect of the mixture equivalence ratio and turbulence intensity on the flame kernel and flow field interlinks in partially premixed natural gas flames. Three jet equivalence ratios of 1, 1.5, and 2 are considered at values of jet velocities in the range from 10 to 20 m/s. This study was done under constant degree of partial premixing. A pulsed Nd: YAG laser is used for the flame ignition, and the turbulent flow field is captured at several time intervals from ignition using two-dimensional Planar Imaging Velocimetry (PIV). The mean flow field doesn't influence with the flame kernel propagation. The turbulent flow field indicates an increase in the global turbulence intensity in flames associated with the kernel propagation in comparison with the isothermal case. The jet equivalence ratio of one enhances the flame kernel propagation and it gives the highest rate of kernel propagation. Increasing the jet equivalence ratio to 1.5 and 2 reduces the intensity of chemical reaction and hence the effect of turbulence becomes the dominant factor effecting the propagation of the flame kernel. At jet velocity of 20 m/s, an early flame kernel extinction is recorded without any respect to jet equivalence ratio. At the early stage of the kernel generation at delay time of 150 μ s, linear correlation between the jet velocity and the kernel propagation is noticed. The chemical reaction is the main factor influences the rate of kernel propagation; it gives nearly 3.5 times the effect of the flow convection to the maximum rate of the flame kernel propagation at jet velocity of 20 m/s and equivalence ratio of one.

Keywords: Flame kernel, Partial premixed flame, PIV, Flow field.

1. INTRODUCTION

The early phase of combustion in spark ignited combustion systems affects the flame propagation and stability, and hence the performance, of the combustion process and the system efficiency. The developing flame kernel represents this phase and is affected by many parameters, such as spark energy, rate of energy release, turbulent flow field and the fuel/air mixing. Previous studies have shown that variations in the initial growth of the flame kernel contribute significantly to cycle-to-cycle variation in engine performance and emissions [1]. The flame kernel has attracted many experimental research groups [2, 3-5] and DNS research groups [4, 6-9] interested in studying flame kernel evolution in turbulent environmental and the main factors that control its characteristics and propagation. Many parameters have been investigated to study their effects on the flame kernel characteristics and propagation, e.g., flame shape, wrinkling and curvature. In the following section a brief review of these studies and their findings are presented and discussed.

Katta et al. [10] reported an experimental and numerical investigation using a unique counter flow diffusion flame with an embedded vortex generator. This study was to understand the local quenching process associated with the vortex-flame interaction in methane diffusion flames. The results show that, the high increase in CH₃ radicals in the strained flame zone depleted the radical pool (such as OH, H, and O) and, hence, the flame is quenched locally. They concluded that this quenching process is different from the quenching observed in steady counter flow flames, where the quenching was due to the gradual reduction in temperature with increasing strain rate. Renard et al. [11] investigated experimentally (using OH PLIF) the flame front of a non-pre-mixed flame interacting with a vortex to study the heat release, extinction and time evolution of the flame surface. They concluded that global intensification or extinction of the flame is characterized by an increase or decrease in flame surface area because of straining. Marley et al. [12] investigated experimentally the interaction of spark-ignited flame kernels with a laminar vortex. They concluded that burning rates for rich flames were decreased, with total flame kernel extinction occurring in extreme cases. They also proved that small flame kernel–vortex interactions are dominated by transient stretch effects and thermo-diffusive stability, in agreement with premixed flame theory. Furthermore, they pointed out that vortex interactions with larger methane–air flame kernels led to slight flame speed enhancements for both lean and rich flame kernels.

Furthermore, Arcoumanis et al. [13] showed that using a small quantity of rich mixture injected near the spark gap can yield to formation of a stable and consistent flame kernel after spark ignition. The function of this local variation in equivalence ratio is to support the flame in a mixture with an overall equivalence ratio as low as 0.39. They concluded that not only the average flame speed could be increased by local injection at all equivalence ratios [14] but also the fluid dynamic effect alone caused overstretching of the flame for the ultra lean homogeneous conditions, while rich local stratification in the vicinity of the spark allowed the suppression of this effect and a reduction of the drivability limit [15]. Roberts et al. [16-18] investigated the added complexity of flame kernel–vortex interactions compared to some earlier planar flame–vortex configuration. They observed experimentally the initial flame kernel–vortex interactions using OH-PLIF in a lean atmospheric-pressure methane–air flame kernel to determine the degree of flame wrinkling and the ability of vortices of varying size and strength to globally quench combustion [16]. The disturbed flame existed in either the flamelet regime (which has a continuous reaction zone) or distributed reaction zone regime (which has a coexistence of reactants and products) is strongly dependent upon: the vortex size, the vortex strength, and the time of the initial flame–vortex interaction. They investigated the global extinction of the flame kernel with large vortex sizes interacting with small flame kernels. In addition to that, they concluded that the localized flame front extinction occurred for a range of vortex sizes and strengths and a range of flame kernel sizes.

Meanwhile, Thevenin et al. [19] and Renard et al. [20] reported an experimental and numerical work of non-premixed flame interacting with a vortex. They investigated the influences of global mixture ratio and vortex velocity on changes in the flame surface. Their study concluded that straining effects are responsible for the extinction of the non-premixed flame front, and the degree of mixing actually increases at the end of the extinction process. They were able to observe the fuel pocket formation, evolution and consumption are another important phenomenon during flame-vortex interactions. In addition to that, the causes for local flame quenching were reported by (Patnaik and Kailasanath [21]) as well. They concluded that these causes happen due to simultaneously high strain and the heat losses in flame-vortex interactions of lean methane/air mixture. Harinath Reddy and John Abraham [22] studied the outcomes of interactions of counter-rotating vortex pairs with developing ignition kernels. They examined quantitatively and qualitatively the evolution of flame surface area during kernel–vortex interaction. They pointed out that flame development is accelerated and the net flame surface area growth rate increased with increasing vortex velocity, besides they proved that increasing the vortex length scale increases the surface growth rate. They noticed when the vortex velocity is high relative to the flame speed, the vortex breaks through the ignition kernel carrying with it hot products of combustion, which accelerates growth of the flame surface area and heat release rates compared to a kernel with no vortex interaction.

Recently, experimental work on the flame kernel structure and propagation in a high turbulent premixed methane flow was performed by Mansour et al. [23] using combined two-dimensional Rayleigh and LIPF-OH techniques. They generated the spark of ignition using pulsed Nd: YAG laser. They investigated four flames at two equivalence ratio of 0.8, and 1, and jet velocity of 6, and 12 m/s.

They showed that the flame kernel structure starts with spherical shape, and then changes gradually to peanut-like, then changes to mushroom-like and finally the turbulence effectively distributes the kernel. They concluded that the trends of the flame propagation, flame radius, flame cross section area, and mean flame temperature are correlated to the jet velocity and equivalence ratio, also lean flames propagate faster.

Based on this review of previous researchs, it is notable that the interaction between the flow field and flame kernel propagation hasn't been investigated experimentally in high turbulent partially premixed flames. Thus, the aim of the present work is to investigate the flow field associated with flame kernel propagation history in partial premixing turbulent flames. The experimental program is devoted to study the effect of the jet equivalence ratio and turbulence intensity on the flame kernel and flow field interlinks in partially premixed natural gas flames. The mean flow field and turbulence intensity are measured using two-dimensional Planar Imaging Velocimetry (PIV), in terms of mean axial velocity and rms. The flow field is first captured for the isothermal field without ignition accompanied, and this could be used as a reference flow field to those flow fields with ignition. The flow field with ignition is recorded after the start of ignition at different delay times. Therefore, the flame kernel-turbulent flow field interaction could be interpreted by the comparison of flow fields of the isothermal and ignited cases.

2. EXPERIMENTAL TECHNIQUE

As shown in Fig.1a, the burner consists of two vertical concentric stainless steel tubes of 6 mm and 10 mm inner diameters and tip thickness of 1 mm. Air is passing through the inner tube while the fuel (natural gas of 95% CH₄ by volume) flows through the annular passage between the inner and outer tubes. The inner tube exit is lower than the exit of the outer tube by a distance L . This distance can be varied to generate different degree of partial premixing. Mixing starts at the exit of the inner tube and continues downstream along the premixing distance L . The burner is sitting at the top of conical turbulence generator as shown in Fig. 1a which is similar to Videto and Santavicca [24] turbulent generator, the flow passes through a narrow slit at a diameter of 45 mm and a slit thickness $b = 0.8$ mm, followed by an inverted cone with 52° base cone angle. The coming flow from the slit provides a ring-like cylindrical shape, which is broken at the inner cone wall to generate a wide range of eddies, which leads to higher turbulence intensity. The turbulence intensity due to this burner concept can be as high as 25% [24]; this is confirmed by the turbulent flow field measurement at the burner exit. The current Planar Imaging Velocimetry technique, explained in details below, requires to image seeding particles within the flow. However, due to the narrow slit dimension of the turbulence generator, it isn't possible to pass all the seeded flow through the slit. Therefore, 10 % of the total air flow rate is used to carry the seeding particles and passes through a central concentric tube with the turbulent generator disk, as shown in Fig. 1a, while the rest of the air flow rate is passed through the slit. Then both streams are mixed inside the cone. Titanium dioxide with a mean diameter of 0.5 μm is used as seeding particles through a fluidized bed seeder.

The interactions between the flame kernel and flow field is investigated at several delay time intervals from ignition, under different jet equivalence ratio and jet velocity. This is based on capturing the turbulent flow field after the ignition at different delay time, namely 150, 300, 500, 1000, 1500, and 2500 μs . These flow fields are compared with flow field without ignition (henceforth to be termed isothermal flow) to identify the effects of the evolving flame kernel. A pulsed Nd:YAG laser (Continuum Surelite II) is used for flame ignition, see Fig.(1-b). Laser ignition provides more stable measurable pulse energy, and overcome the problems of the effects of spark electrodes on the flame structure, as well as heat loss to the electrodes. The laser provides a beam of 6 mm diameter at 1064 nm with 230 mJ and is focused to a beam of waist radius of 5.6 μm using spherical lens of 50 mm focal length.

As shown in Fig.(1-b), the flow field is measured using two-dimensional Particle Imaging Velocimetry (PIV) technique, of two head Nd:YAG laser with pulse energy of 50 mJ at the second harmonic of 532 nm. The camera is HiSense MkII PIV CCD cameras (model C8484-5205CP) with 1280 x 1024 CCD light sensitive array and equal number of storage cells. The objective of the camera is covered with interference filters at 532 nm with a bandwidth of 10 nm. The laser pulse duration is 6 ns and the inter-pulse delay between the two laser heads is controlled according to the flow velocity with a minimum of 0.2

μ s for supersonic flow. The laser sheet is created by sheet forming optics that produces expanding laser sheet. Timing between the laser ignition, the PIV laser sheet forming and the camera capturing was controlled by 4 channel Stanford Research DG535 pulse delay generator and monitored with a Tektronix 4 channel 200 MHz oscilloscope. The PIV images were processed using an adaptive window offset cross-correlation algorithm implemented in a commercial analysis package (Dantec Dynamic Studio V 2.30). The final interrogation window was 32×32 pixels with a 50% window overlap, resulting in a spatial resolution 1.5 mm and vector spacing of 0.5 mm.

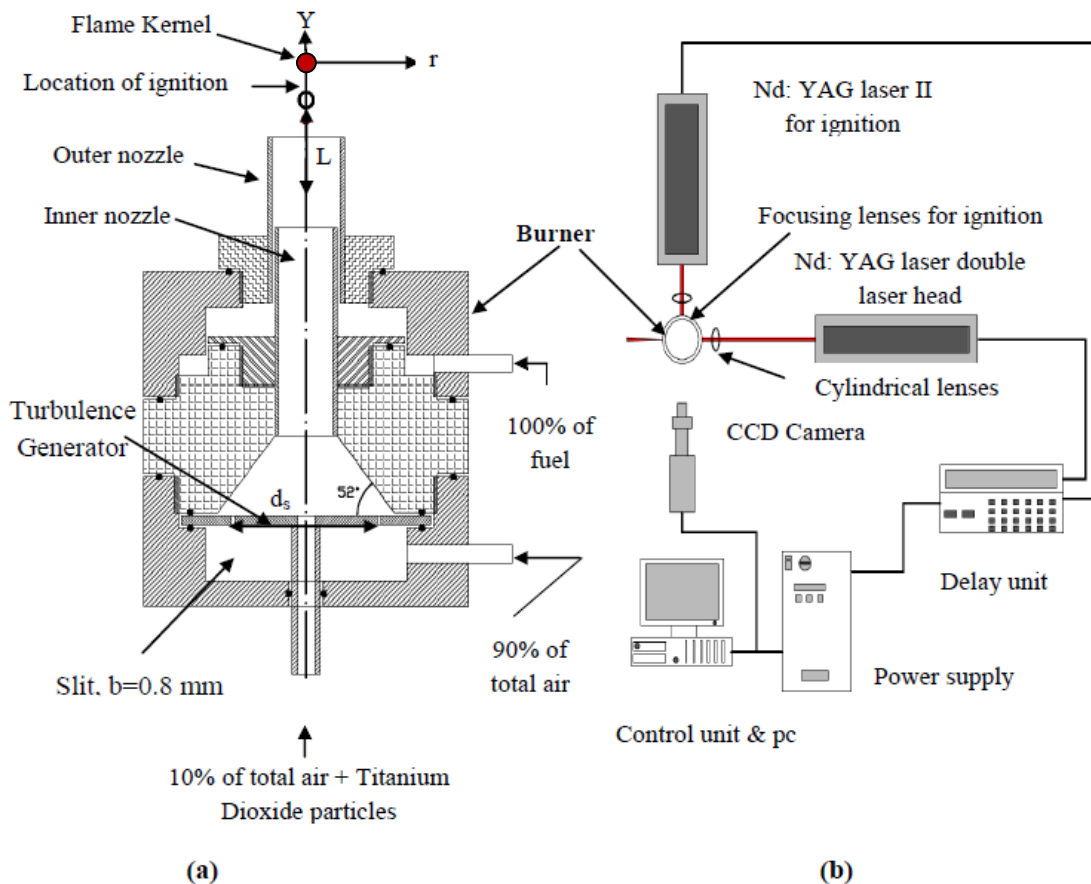


FIGURE 1: a) The burner, b) The experimental set up.

3. FLAME STABILITY AND SELECTED CONDITIONS

Flame extinction can be approached by either increasing the jet velocity for the same fueling rate or reducing the equivalence ratio at the same jet air velocity. In the present work the degree of partial premixing is fixed where the premixing length L is kept constant at $L/D = 2$ for all cases, where D is the inner diameter of the outer burner tube. Figure 2 illustrates the stability characteristics of the burner, where the stability point is achieved via gradual decrease of the fuel flow until the flame blows off, while preserving the air flow rate constant. The results are presented as a relation between the jet velocity (U_j) and the jet equivalence ratio (Φ_j). The results depicted in Fig. 2 shows that the higher the jet velocity, the higher the corresponding jet equivalence ratio required for stable flames.

In relevance with the stability limit, the flame kernel and the turbulent flow fields are investigated at three jet equivalence ratio of 1, 1.5 and 2. For each equivalence ratio, five different jet velocities are applied and investigated beginning from 10 m/s to 20 m/s with increasing step of 2.5 m/s, see Fig. 2. The flow

conditions are listed in Table 1. The flames are selected on the unstable region, and the flame kernels are ignited and propagated after each laser pulse. Since this is unstable flame region, this allows the recording ability of the flow fields at several times from the ignition during the flame kernel propagation, without the need to shut down the flame. The flow fields of the previous flames are also examined without ignition (isothermal flow conditions) to be used as references of comparison with those flow fields accompanied by flame kernel.

Uj(m/s)	$\Phi_j=1$	$\Phi_j=1.5$	$\Phi_j=2$
10	√	√	√
12.5	√	√	√
15	√	√	√
17.5	√	√	√
20	√	√	√

Table 1: The selected flames conditions

*The flame designation is $F\Phi_j-U_j$, where, the symbol Φ_j after F indicates the jet equivalence ratio, while the second number represents the jet velocity. For example, F1-10, it means the jet equivalence ratio equals 1 and jet velocity equals 10 m/s. The isothermal case is indicated by adding a superscript iso to the previous acronym, like $F2-10^{iso}$, it means at those flow conditions the turbulent flow field is recorded without ignition.

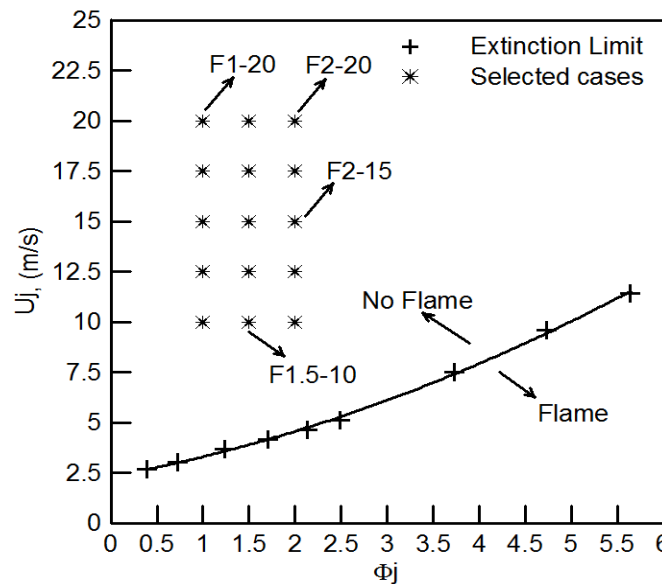


FIGURE 2: Stability limit and the selected flame conditions

4. RESULTS AND DISCUSSION

The contours of the normalized mean axial velocity U/U_j of isothermal jet flow and the ignited cases of flame F2-10 are illustrated in Fig. 3a at several time intervals from ignition, [the isothermal case is located at the left of the figure while those on the right are the time history of the mean velocity fields of the ignited cases]. As shown for the mean flow field, there is no any difference between the isothermal case and the ignited cases at any delay time from the ignition. For the isothermal and the ignited cases, the flow field is featured by a central core region extending to a nearly axial distance of $2D$ (D is the inner diameter of the outer nozzle), with axial velocity of nearly $U/U_j=1.2$. The core flow region is surrounded by annular mixing region, which merges downstream the end of the potential core region. This result demonstrates that the flame kernel propagation has no effect on the mean flow field.

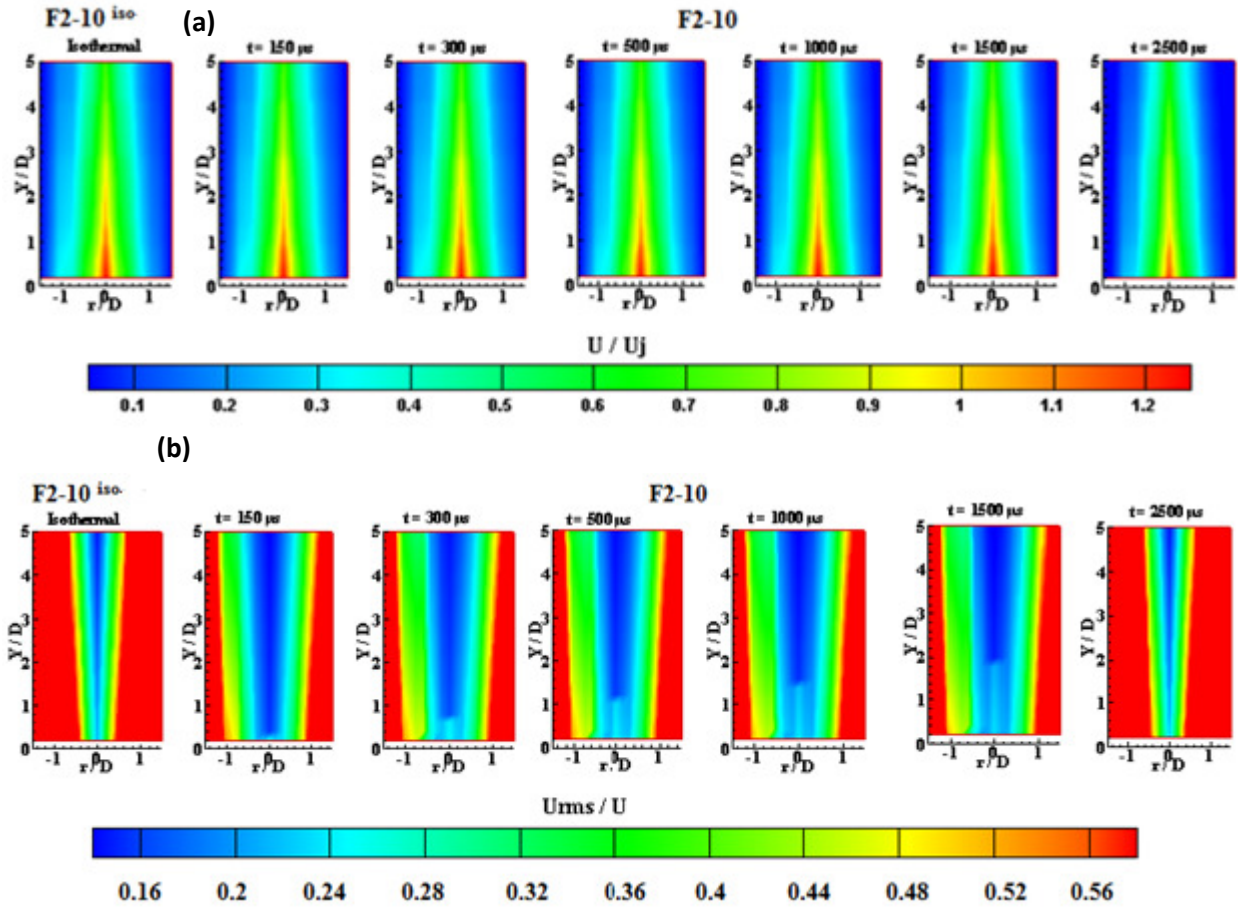


FIGURE 3: (a) Contours of the normalized mean axial velocity (U/U_j) for isothermal, at the left hand side and the ignition cases at several time intervals from ignition in flame F2-10, at the right of the isothermal case, (b) Contours of the normalized rms (U_{rms}/U) for isothermal, at the left hand side and the ignition cases at several time intervals from ignition in flame F2-10.

On the other hand, as shown in Fig. 3b the contours of the turbulence intensity in terms of U_{rms}/U , shows a significant difference between the isothermal and the ignited cases. This can be seen by the higher turbulence intensity along with the jet centerline in case of the ignited cases at any delay time from the ignition with respect to the isothermal case. This central region of the higher turbulence intensity is propagated in the range of the delay of 150 to 1500 μs , and shows a maximum propagation axial distance at 1500 μs . After this time the turbulent flow field returns again to the original turbulence state at time delay of 2500 μs , as the isothermal case (see the first and the last contours of Fig. 3b). This result indicates that the flame kernel affects the turbulent flow field. Other feature of the turbulence intensity field associated with the flame kernel propagation is the increase of the width of the radial distribution of the turbulence intensity in the range of U_{rms}/U (from 0.16 to 0.56), this turbulence intensity range is spanning a narrow radial distance in the isothermal case with the comparison of the ignited cases at any axial distances. This means that the flame kernel propagation leads to the redistribution the turbulent kinetic energy.

Figure 4 illustrates the radial profiles of the turbulence intensity of flame F2-10 at delay time of 1000 μs at three axial distances, namely at the point of the sudden decay of turbulence intensity which can be taken as a trace of flame kernel propagation, X , while the other two locations upstream and downstream X , by 2 mm, $X-2$, $X+2$, respectively. The close inspection of the profiles shows that the turbulence intensity is

relatively high along the flame centerline at X-2 and X. More outward displacement from the jet centerline, the turbulence intensity showed a slight decrease reaching a minimum turbulence intensity point, and this indicates that the kernel centerline is associated with higher turbulence intensity. Beyond the radial location of the point of minimum turbulence intensity, the turbulence intensity starts to increase and merges with the profiles of the turbulence intensity of the axial position at X+2. Where the turbulence intensity profile at X+2 shows a minimum value at the jet centerline, which is similar to the ordinary jet flow. This indicates at the axial position of X+2, the kernel is extinguished, which indicates the reasons behind the radial stretching of the turbulence intensity profiles in the case of the ignited flame kernel with the comparison to the isothermal one.

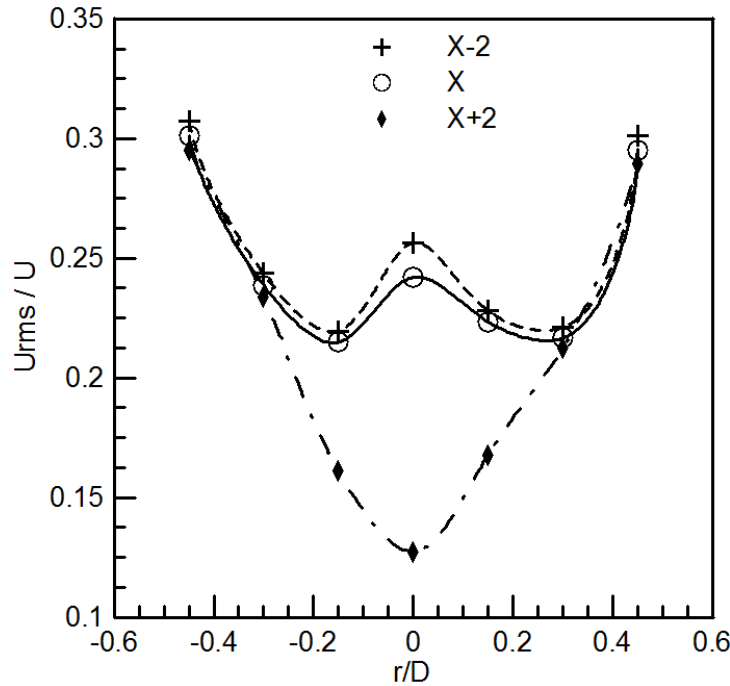


FIGURE 4: Radial distribution of axial turbulence intensity at different axial locations: upstream the flame kernels limit X-2, at the flame kernel limit X, and at downstream the kernel X+2 of flame F2-10 at delay time = 1000 μ s.

Fig. 5 shows the centerline turbulence intensity for the jet equivalence ratio of one and jet velocity of 10 m/s at different time of delay from the ignition, with the comparison with the isothermal case. As seen as the flame kernel propagates as it delays the steep decay point of the turbulence intensity, and by this way the flame kernel could be traced. At jet velocity of 10 m/s, increasing the jet equivalence ratio from 1 to 1.5 and 2 shows similar qualitative turbulence intensity change, as compared to the corresponding isothermal cases, see Fig. 6. To quantify the effect of the jet equivalence ratio on the turbulence intensity accompanied with the flame kernel propagation. This turbulence intensity along the jet centerline for the three equivalence ratios at delay time of 1000 μ s and jet velocity of 10 m/s is illustrated in Fig.7. All of these centerline turbulence intensities are compared to the isothermal case in the same figure. In general, centerline turbulence intensity of the isothermal case shows nearly linear decrease in turbulence intensity along the axial distance. While, for the three equivalence ratios of the ignited cases, the centerline turbulence intensity is noticed to be higher at the early axial distance, which also shows a mild decrease in the turbulence intensity along with the increase in the axial distance. This mild decline in the turbulence intensity is changed into a steep decrease in the turbulence intensity to a lower level of turbulence intensity; but this level is still higher than those recorded in the isothermal case.

As mentioned before, the axial location of the steep decrease in the centerline turbulence intensity can be taken as an indication of the flame kernel propagation. The high turbulence regime may be occurred due to flame kernel fluctuation in this region and this should be associated with large rms and consequently high turbulence intensity. In addition, the interaction between the flame kernel and flow field likely causes disturbance and hence another factor affects the turbulence intensity. Thus, the position of the decrease

of the turbulence intensity can be used as the mean position of the flame kernel, (this will be demonstrated later in the section of the rate of flame kernel propagation).

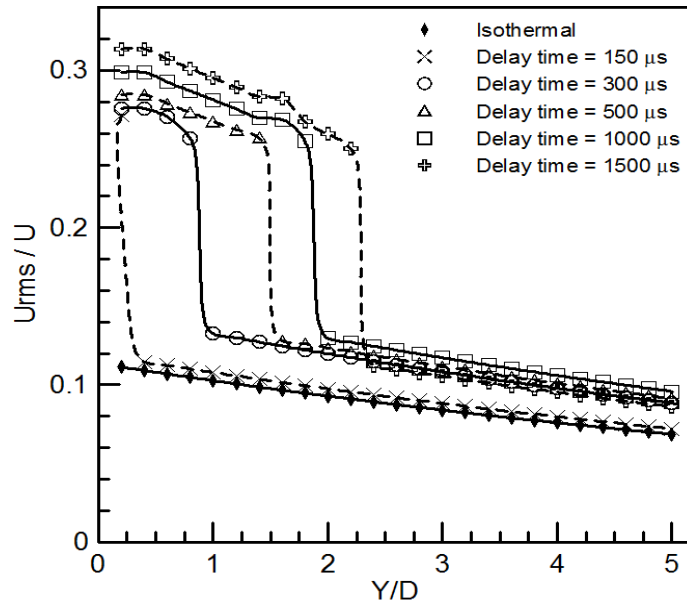


FIGURE 5: The centerline U_{rms}/U for F1-10 at different time of delay and the corresponding isothermal case

As shown in Fig. 7, the jet equivalence ratio of 1 gives the highest flame kernel propagation while it decreases by increasing the equivalence ratio. This is consistent with variation of the flame speed with the gradient in the equivalence ratio. This reflects the effect of fuel-air chemistry on the flame kernel propagation, where the partial premixed mixture with jet equivalence ratio of 1 sustains the flame kernel propagation. This could be explained on the basis of the higher chemical reaction rate of the stoichiometric mixture to withstand the turbulence effect. On the other hand, increasing the jet equivalence ratio decreases the chemical reaction rate and hence the effect of turbulent on the flame kernel becomes predominate, this affects the kernel propagation and its rate.

With the respect to the flame kernel propagation and the rate of propagation, Fig. 8 shows a comparison between our results and those results of Mansour et al [23]. The results of Mansour et al. [23] are based on using a combined two-dimensional Rayleigh and LIPF-OH technique. Where, the average axial locations of the flame kernel center, obtained from all 200 images of LIF-OH measured in each flame. The results show an excellent agreement between our data and the compared ones up to delay time of 300 μs , while after this delay time the two trends are qualitative similar with a slight increase in our kernel propagation, and this is believed due to the slight increase in our selected jet velocity by 0.5 m/s, which enhances the kernel propagation, as well as, the results of Mansour et al [23], were performed on a premixed mixture.

The effect of both jet velocity and jet equivalence ratio on the flame kernel propagation and the rate of the flame kernel propagation can be understood from Figs. 9 and 10, respectively. In Fig. 9, the flame kernel propagation distance Z in mm is represented on the vertical axis versus the jet velocity on the horizontal axis at each delay time from the ignition. The results indicate that the flame kernel propagation increases with increasing the jet velocity at any delay time from ignition, and this is attributed to the higher convection effect of the flow with increasing the jet velocity.

At early stage of the flame kernel generation at time lag of 150 μs a linear correlation between the jet velocity and flame kernel propagation is recorded for the three jet equivalence ratio. Beyond this time lag of 150 μs , a deviation from the linear correlation between the jet velocity and the kernel propagation is noticed and the nonlinearity increases with increasing the delay time. This may be explained based on the results of Mansour et al [23], where the shape of the flame kernel at the early delay time is not affected by turbulence and hence this reduces the effect of turbulence level on the flame kernel propagation at the early time of flame kernel generation. At this early time stage the flame kernel is

almost spherical. After some more time the flame kernel shape is corrugated and takes different shape, and hence the effect of the turbulence intensity of the flow field is predominate and the flame kernel boundaries is affected more by the turbulence eddies.

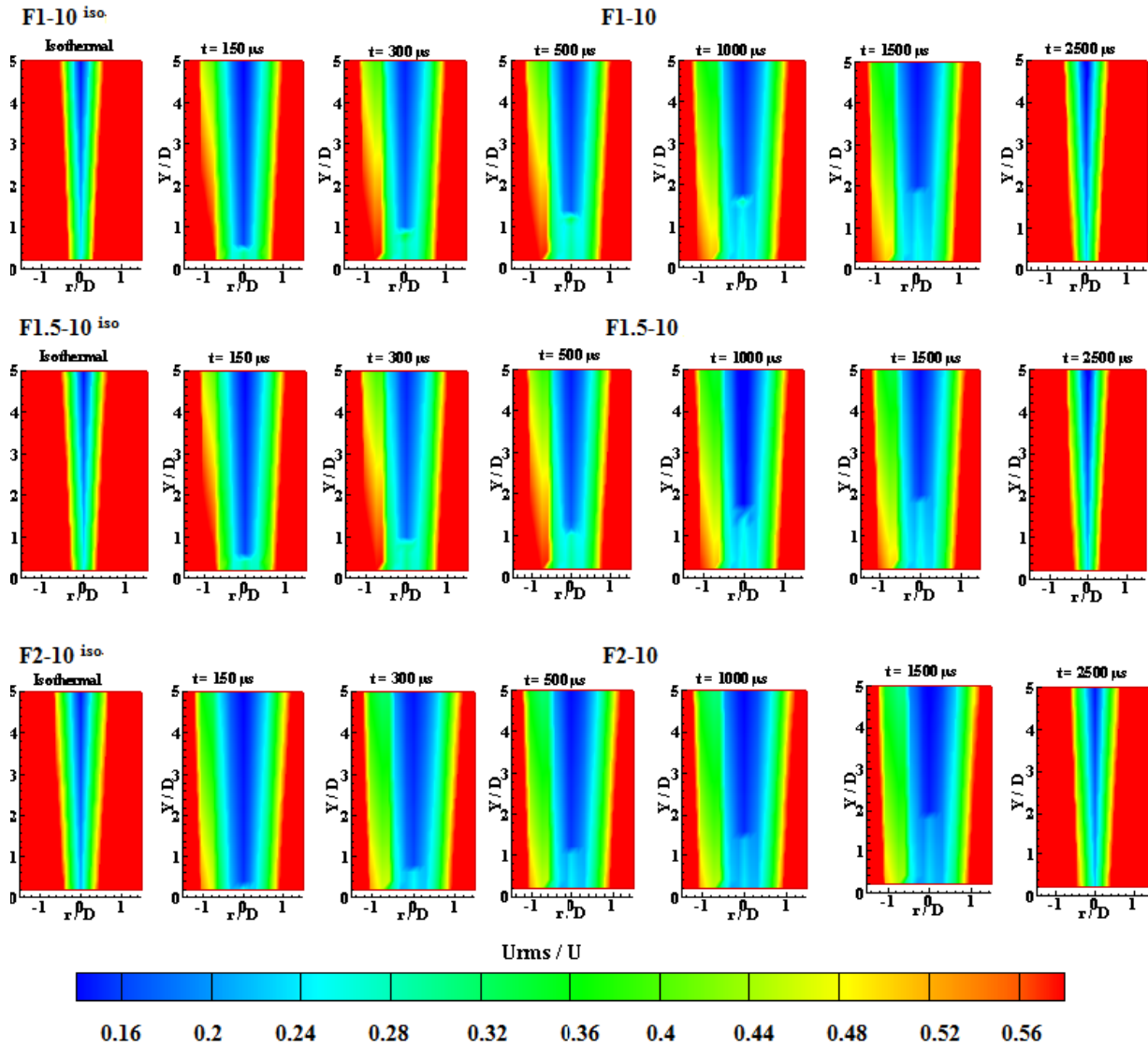


FIGURE 6: Contours of the axial turbulence intensity U_{rms}/U of flame F1-10, flame F1.5-10 and flame F2-10 (from top to bottom, respectively)

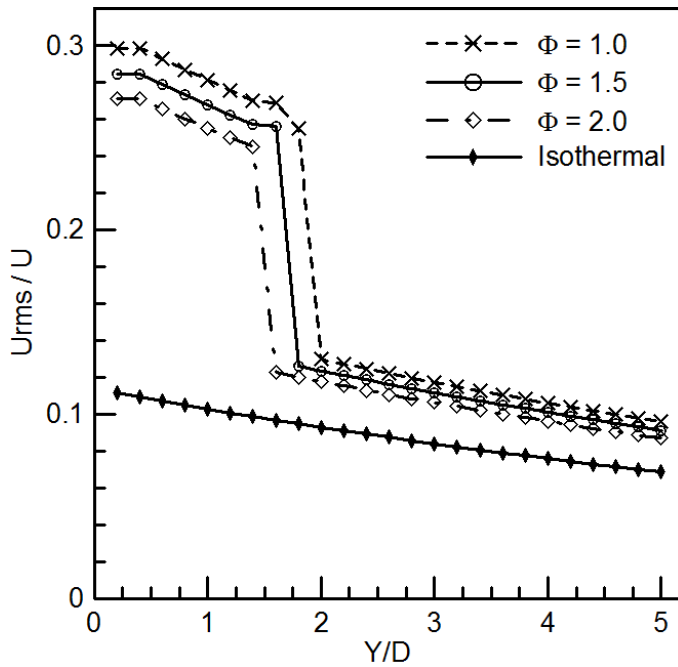


FIGURE 7: Centerline axial turbulence intensity at $U_j = 10$ m/s with $\Phi_j = 1, 1.5,$ and $2,$ at delay time of $1000 \mu\text{s}$ with comparison to the isothermal case.

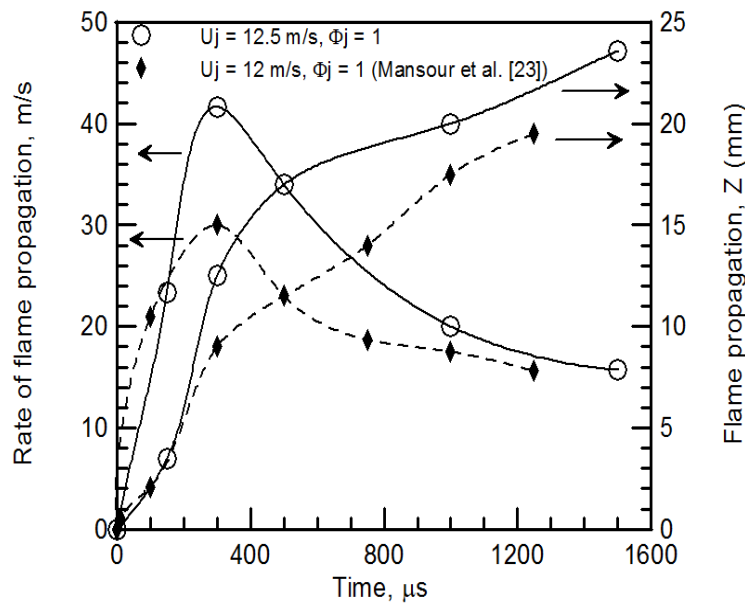


FIGURE 8: The flame kernel propagation and rate of flame kernel propagation at $\Phi_j = 1,$ and $U_j = 12.5$ m/s, compared to Mansour et al [23], at $\Phi_j = 1,$ and $U_j = 12$ m/s.

The above results can be reflected on the flame kernel propagation rate, see Fig. 10, the data provides an illustration of the flame kernel propagation rate in m/s (vertical axis) at different delay times presented on the horizontal axis. The results show that the rate of flame propagation increases with respect to the time in steep manner till reaching a maximum rate at nearly $300 \mu\text{s}$ for all jet velocity. This maximum rate increases with increasing the jet velocity due to the higher convection effect. After this point of maximum

rate, the flame kernel propagation rate is attenuated with increasing the time lag. This decay in the rate of flame propagation is very clear at the higher jet velocity see jet velocities of 17.5 and 20 m/s in Fig. 10. This indicates that increasing up to these high jet velocities of 17.5 and 20 m/s, increases the turbulence intensity to a level which leads to the weakness of the chemical reaction, where the chemical reaction can't withstand these high rates of reactants. At the same time the higher the jet velocity leads to more local turbulence intensity in the location of the kernel, which in turn increases the heat dissipated to the surrounding and the kernel extinction occurs. This could be highlighted by the relative early flame kernel extinction at the jet velocity of 20 m/s without any relevance to the mixture equivalence ratio. If the maximum rate of flame kernel propagation is normalized by the exit jet velocity, it will indicate the effect of the chemical reaction for the flame kernel rate of propagation. At the jet velocity of 20 m/s and jet equivalence ratio of 1, the ratio of the maximum rate of flame kernel propagation to the exit jet velocity is nearly 3.5; this proves that the chemical reaction enhances the rate of flame kernel propagation more than the coming from the convective effect of the flow field.

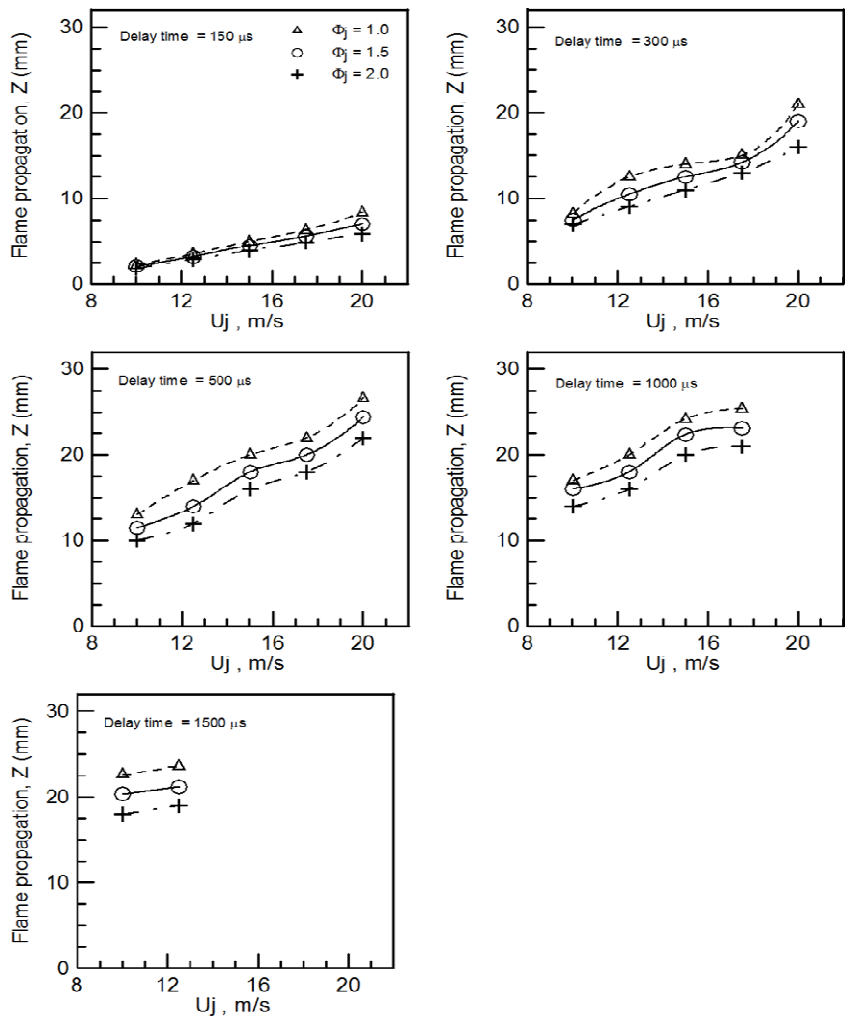


FIGURE 9: Flame kernel propagation at $\Phi_J = 1, 1.5$ and 2 for different delay times.

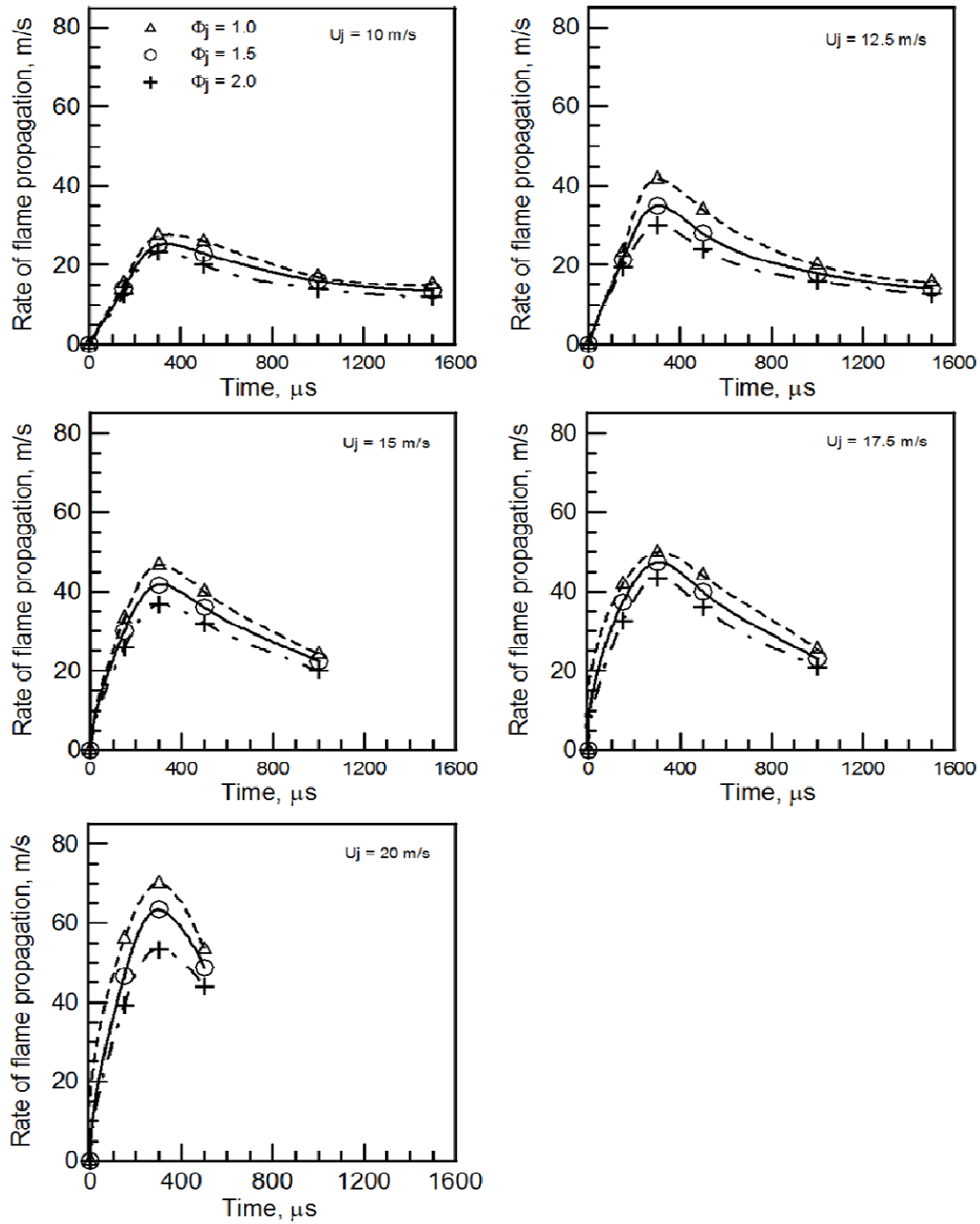


FIGURE 10: Rate of Flame kernel propagation at $\Phi_j = 1, 1.5$ and 2 for different jet velocities.

5. CONCLUSIONS

An experimental work is conducted on the flame kernel propagation of partial premixed natural gas turbulent flames under a constant degree of partial premixing. The study is oriented to study the effect of jet equivalence ratio and jet velocity on the flow field-flame kernel interaction. The mean flow field and turbulence intensity are measured using two-dimensional Planar Imaging Velocimetry (PIV). The flow field is captured for the isothermal field without ignition in order to be used as a reference to those flow fields with flame kernel. The flow field with ignition is recorded after the start of ignition at different delay times. The data show that the mean flow field isn't affected by the flame kernel if it is compared to the isothermal one. It is found that the centerline turbulence intensity increases during the flame kernel propagation, and then followed by a sudden decrease. The flame kernel propagation and its rate in the stoichiometric flames are occurred at higher rates compared to the richer flames. This is consistent with the flame speed

International Journal of Applied Science (IJAS), Volume (3): Issue (2): 2012

data where the maximum flame speed occurs at the stoichiometric cases. This leads to more significant effect of turbulence on the flame kernel propagation at richer conditions. During the early period of the flame kernel generation, within the first 150 μ s period, a linear correlation between the jet velocity and flame kernel propagation is recorded for all equivalence ratios. Beyond this period of 150 μ s, a deviation from the linear correlation between the jet velocity and the kernel propagation is noticed and the nonlinearity increases with increasing the delay time. This indicates that flame kernel propagation is accelerated. Moreover, increasing the jet velocity up to nearly 17.5 m/s and more, increases the turbulence intensity to a limit which weakens the chemical reaction, which can't withstand this higher rates of reactants. The relative early flame kernel extinction at the jet velocity of 20 m/s is occurred without any relevance to the value of jet equivalence ratio.

6. ACKNOWLEDGEMENTS

This work is financially supported by the joint project between Cairo University, Egypt, and North Carolina State University, USA. The project title is "Computational and Experimental Studies of Turbulent Premixed Flame Kernels". The project ID is 422.

7. FUTURE WORK

To go more depth about the flame kernel and flow field interaction, planar laser-induced fluorescence (PLIF) and stereoscopic particle image velocimetry (PIV) will be applied at 10 KHz repetition-rate to acquire time-resolved of the flow field flame kernel interaction.

8. REFERENCES

- [1] R.R. Maly, in: J.C. Hilliard, G.S. Springer (Eds.), "Flow and Combustion in Reciprocating Engines," *Plenum Press, New York*, 1983.
- [2] C.F. Kaminski, J. Hult, M. Alden, S. Lindenmaier, A. Dreizler, U. Mass, M. Baum, "Complex turbulence/chemistry interactions revealed by time resolved fluorescence and direct numerical simulations," *Proceedings of the Combustion Institute* 28:399–405(2000).
- [3] A. Dreizler, S. Lindenmaier, U. Maas, J. Hult, M. Alden, C.F. Kaminski, "Characterization of a spark ignition system by planar laser induced fluorescence of high repetition rates and comparison with chemical kinetic calculations," *Applied Physics B*70:287–294 (2000).
- [4] S. Gashi, J. Hult, K.W. Jenkins, N. Chakraborty, R.S. Cant, C.F. Kaminski, "Curvature and wrinkling of premixed flame kernels – comparisons of OH PLIF and DNS data," *Proceedings of Combustion Institute* 30:809–817 (2005).
- [5] C.C. Huang, S.S. Shy, C.C. Liu, A. Yan, "A transition on minimum ignition energy for lean turbulent methane combustion in flamelet and distributed regimes," *Proceedings of the Combustion Institute* 31:1401–1409(2007).
- [6] K.W. Jenkins, R.S. Cant, "Curvature effects on flame kernels in a turbulent environment," *Proceedings of the Combustion Institute* 29:2023–2029(2002).
- [7] D. Thevenin, O. Gicquel, J. de Charentenay, R. Hilbert, D. Veynante, "Two versus three dimensional direct simulations of turbulent methane flame kernels using realistic chemistry," *Proceedings of the Combustion Institute* 29:2031–2039 (2003).
- [8] N. Chakraborty, M. Klein, R.S. Cant, "Stretch effects on displacement speed in turbulent premixed flame kernels in the thin reaction zones regime," *Proceedings of the Combustion Institute* 31: 1385–1392(2007).
- [9] K.W. Jenkins, M. Klein, N. Chakraborty, R.S. Cant, "Effects of strain rate and curvature on the propagation of a spherical flame kernel in the thin reaction zones regime," *Combustion and Flame* 145:415–434 (2006).
- [10] V.R. Katta, K.Y. Lisu, and W.M. Roquemore, "Local Extinction in an unsteady methane-air jet diffusion flame," *Proceedings of the Combustion Institute* 27:1121-1129 (1998).
- [11] P.H. Renard, J.C. Rolon, D. Thevenin, , and S. Candel, "Investigations of heat release, extinction, and time evolution of the flame surface, for a non-premixed flame interacting with a vortex," *Combustion and Flame* 117:189–205 (1999).

- [12] S.K. Marley, S.J. Danby, W.L. Roberts, M.C. Drake, T.D. Fansler, "Quantification of transient stretch effects on kernel–vortex interactions in premixed methane–air flames," *Combustion and Flame* 154 (2008) 296–309.
- [13] C. Arcoumanis, D.R. Hall, and J. H. Whitelaw, "An approach to charge stratification in lean-burn spark-ignition engines," *SAE technical paper* 941878 (1994).
- [14] C. Arcoumanis, D.R. Hall, and J.H. Whitelaw, "Optimizing local charge stratification in a lean-burn spark ignition engine," *Proc. Instn. Mech. Engrs, Part D: J. Auto. Eng.* 211:145–154(1997).
- [15] C. Arcoumanis, M.R. Gold, J.H. Whitelaw, and H.M. Xu, "Local mixture injection to extend the lean limit of spark-ignition engines," *Exper. Fluids* 26:126–135 (1999).
- [16] D.A. Eichenberger, W.L. Roberts, "Effect of unsteady stretch on spark-ignited flame kernel survival," *Combustion and Flame* 118:469–478(1999).
- [17] Y. Xiong, W.L. Roberts, M.C. Drake, T.D. Fansler, "Investigation of pre-mixed flame-kernel/vortex interactions via high-speed imaging," *Combustion and Flame* 126:1827–1844 (2001).
- [18] Y. Xiong, W.L. Roberts, "Observations on the interaction between a premixed flame kernel and a vortex of different equivalence ratio," *Proceedings of the Combustion Institute.* 29:1687–1693(2002).
- [19] D. Thevenin, P.H. Renard, J.C. Rolon, and S. Candel, "Extinction processes during a non-premixed flame / vortex interaction," *Proceedings of the Combustion Institute.* 27:719–726 (1998).
- [20] P.H. Renard, J.C. Rolon, D. Thevenin, and S. Candel, "Wrinkling, pocket formation and double premixed flame interaction processes," *Proceedings of the Combustion Institute.* 27:659–666 (1998).
- [21] G. Patnaik, and K. Kailasanath, "A computational study of local quenching in flame-vortex interactions with radiative losses," *Proceedings of the Combustion Institute.* 27:711–717 (1998).
- [22] H. Reddy and J. Abraham, "A Numerical Study of Vortex Interactions with Flames Developing from Ignition Kernels in Lean Methane/Air Mixtures," *Combustion and Flame* 158 (2011) 401–415.
- [23] M.S. Mansour, , N. Peters, L.U. Schrader, "Experimental study of turbulent flame kernel propagation," *Experimental Thermal and Fluid Science.* 32:1396–1404(2008).
- [24] B.D. Videto, D.A. Santavicca, "A turbulent flow system for studying turbulent combustion processes," *Combustion Science and Technology* 76 (1991) 159–164.

A Thresholding Method to Estimate Quantities of Each Class

Kenta Azuma

Graduate School of Science and Engineering
Saga University
Saga City, 840-8502, Japan

azuma@imageone.co.jp

Kohei Arai

Graduate School of Science and Engineering
Saga University
Saga City, 840-8502, Japan

arai@is.saga-u.ac.jp

Ishitsuka Naoki

Country Ecosystem Informatics Division
National Institute for Agro-Environmental Sciences
Tsukuba City, 305-8604, Japan

isituka@niaes.affrc.go.jp

Abstract

Thresholding method is a general tool for classification of a population. Various thresholding methods have been proposed by many researchers. However, there are some cases in which existing methods are not appropriate for a population analysis. For example, this is the case when the objective of analysis is to select a threshold to estimate the total number of data (pixels) of each classified population. In particular, If there is a significant difference between the total numbers and/or variances of two populations, error possibilities in classification differ excessively from each other. Consequently, estimated quantities of each classified population could be very different from the actual one.

In this report, a new method which could be applied to select a threshold to estimate quantities of classes more precisely in the above mentioned case is proposed. Then verification of features and ranges of application of the proposed method by sample data analysis is presented.

Keywords: Thresholding, Classification, Quantity of a class, Counting accuracy, Synthetic aperture radar.

1. INTRODUCTION

Thresholding method is a general tool for classification of a population. This method is one of the picture binarization techniques. Various thresholding methods have been proposed by many researchers. These thresholding methods were listed and evaluated by Dr. Sahoo and Dr. Wong in the field of image processing [1]. These methods were categorized as point dependent techniques[2][3][4][5][6][7], region dependent techniques[8][9][10][11][12] and multi-thresholding[13][14][15]. In the field of classical image processing “Uniformity index” and “Shape index” are used to evaluate an analysis and a threshold. These indexes can evaluate for visibility and legibility of a character and an object in a classified image. By contrast, “overall accuracy” is used to evaluate in field of classification of many applications. Especially, some methods proposed by Dr. Otsu [16][17], Dr. Kittler et al. [18][19] and Dr. Kurita et al. [20][21] have a simple algorithm and are easy for data handling and can get high accuracy results. Hence, these techniques have been applied for a lot of classification analysis. These are effective methods for increasing the overall accuracy of analysis. However, there are some cases in which these methods are not appropriate for a population analysis.

For example, this is the case when the objective of analysis is to select a threshold to estimate the total number of data (pixels) of each classified population. In particular, If there is significant

difference between the total numbers and/or variances of two populations, error possibilities in classification differ excessively from each other. Consequently, estimated total number of each classified population could be very different from the actual one.

For the field of remote sensing, there are many cases which the area of a target is estimated using a satellite data [22][23][24][25]. The purpose of these analyses is just to estimate the total number of data (pixels) of each classified population.

In this report, authors propose a new method which could be applied to specify a threshold to estimate the quantity of data more precisely in the above mentioned case. And this method is applied for estimation of planting area of rice paddy using a synthetic aperture radar (hereinafter referred to as SAR) data. Then some advantageous effects of the proposed method are shown.

2. METHOD FOR THRESHOLD SELECTION

Lets us consider the most appropriate threshold for classifying pixels from an image represented in gray scale. Of course, the definition of the most appropriate threshold depends on its purpose. In this paper, we propose a threshold to estimate the quantities, total amount of data, of each classified population most precisely.

In the past, purpose of most thresholding methods was to decrease the number of misclassifications. This analysis is to improve the overall accuracy of a classification. However, the most appropriate threshold to estimate the quantities of each classified population differs from a threshold to make the overall accuracy highest. For example, even if the overall accuracy is high, it could happen that an estimated quantity differs from true value grossly when there is an excessive difference between the parameters including total amount of pixels and deviations of each class. On the contrary, even if there may be many misclassifications, estimated quantities of each class could be very similar to true values when the numbers of misclassifications of each class are very similar to each other. Therefore the most appropriate threshold to estimate quantities of each class is a threshold which can minimize the difference between the numbers of misclassifications of each class.

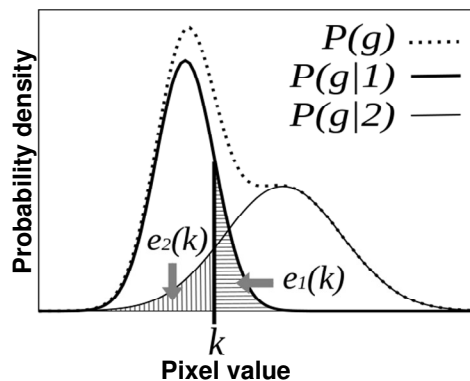


FIGURE 1: Probability density functions and misclassifications of each class

Let the pixels of given image be represented in gray levels $g = \{1, 2, \dots, L\}$. The histogram of the gray levels in this image is denoted by $h(g)$. Then the probability density function of gray levels is given by $p(g) = h(g)/N$, where N is the total number of pixels in the image. Now supposing that the $p(g)$ is a mixed population compounded of class 1 ($i=1$) and class 2 ($i=2$), distributions of each class are denoted by $p(g|i)$ and a prior probabilities by P_i . The probability density function of gray levels is also given by

$$p(g) = \frac{h(g)}{N} = \sum_{i=1}^2 P_i p(g|i) . \quad (1)$$

These parameters are shown in Figure 1. Where Broken line is the distribution of input data, Solid lines are distributions of each class estimated by optimization and Striped areas, $e_1(k)$ and $e_2(k)$ denote misclassifications should be considered at first. Supposing that the pixels are categorized into two classes by threshold at level k , pixels not more than threshold k can be classified into class 1. On the other hand, pixels which are more than threshold k can be classified into class 2. In this case, the total number of class 1 and class 2 are given by

$$\begin{aligned} n_1(k) &= N \sum_{g=1}^k p(g) = N \sum_{g=1}^k \sum_{i=1}^2 P_i p(g|i) \\ n_2(k) &= N \sum_{g=k+1}^L p(g) = N \sum_{g=k+1}^L \sum_{i=1}^2 P_i p(g|i) \end{aligned} \quad (2)$$

The number of pixels belonging to class 1 which are misclassified into class 2 is denoted by $e_1(k)$. And the number of pixels belonging to class 2 which are misclassified into class 1 is denoted by $e_2(k)$. These are given by

$$\begin{aligned} e_1(k) &= N \sum_{g=k+1}^L P_1 p(g|1) \\ e_2(k) &= N \sum_{g=1}^k P_2 p(g|2) \end{aligned} \quad (3)$$

Then, an assumption that $e_1(k)$ and $e_2(k)$ are approximated when the threshold k is equal to the value τ is introduced. In other words, the value τ can minimize the criterion function

$$\varepsilon(k) = (e_1(k) - e_2(k)) . \quad (4)$$

In this case, the total number of the pixels classified into class 1 can be evaluated as

$$\begin{aligned} n_1(\tau) &= N \sum_{g=1}^{\tau} (P_1 p(g|1) + P_2 p(g|2)) \\ n_1(\tau) &\approx N \sum_{g=1}^{\tau} P_1 p(g|1) + N \sum_{g=\tau+1}^L P_1 p(g|1) \\ n_1(\tau) &\approx N \sum_{g=1}^L P_1 p(g|1) \\ n_1(\tau) &\approx NP_1 \end{aligned} \quad (5)$$

Thus, the total number of pixels classified into class 1 is very close to the true value. Similarly the total number of the pixels classified into class 2 can be evaluated as

$$n_2(\tau) \approx NP_2 . \quad (6)$$

Also the total number of pixels classified into class 2 is very close to the true value.

As a result, using the threshold τ which can minimize the difference between the numbers of misclassification pixels of class 1 and class 2, the quantity of classified pixels can be approximated to the true value. In order to compute the threshold τ which can minimize the criterion function $\varepsilon(k) = |e_1(k) - e_2(k)|$, following procedures are needed.

- To formulate a histogram and a probability density function from an input image.
- To optimize a histogram to a mixed population.
- To calculate the threshold τ which can minimize the criterion function from the mixed population.

In order to optimize a histogram and the threshold τ an optimization technique (e.g., the steepest descent method, the downhill simplex [26], the simulated annealing [27]) has to be used.

The result of classification is evaluated using a confusion matrix first. The confusion matrix is shown in Table 1, where, n is the number of evaluated pixels, the first subscript denotes a class number of the classified image, the second subscript denotes a class number of the correct classification result and a symbol “+” denotes summation. In particular, n_{11} and n_{22} denote the number of pixels which were classified correctly. n_{12} and n_{21} denote the number of pixels which were classified as false. n_{i+} denote the number of pixels which were classified into class i . And N_i denotes the correct number of pixels belonging to class i .

TABLE 1: Confusion matrix for evaluation

		True Data		Σ
		Class1	Class2	
Classifier	Class1	n_{11}	n_{12}	n_{1+}
	Class2	n_{21}	n_{22}	n_{2+}
Σ		N_1	N_2	N

After evaluation by the confusion matrix, typically the result of classification is evaluated using the overall accuracy O , the producer's accuracy P and the user's accuracy U [28]. These accuracies are given by

$$O = \frac{\sum_{i=1}^2 n_{ii}}{N}, \quad P_i = \frac{n_{ii}}{N_i}, \quad U_i = \frac{n_{ii}}{n_{i+}} \quad (7)$$

These accuracies are useful to evaluate a result of classification. However those may not be suitable for evaluation of a threshold value. For example, this is the case when the numbers of each class differ widely. In this case, an accuracy of majority class becomes dominant in the overall accuracy. And an accuracy of minority class is neglected. In the result, the greater the number of estimated pixels which are classified to the majority class, the greater the overall accuracy is increased. So the overall accuracy is not suitable to evaluate a threshold value. Furthermore, the producer's accuracy is improved when a threshold changes in a direction which classifies pixels more into a target class. The user's accuracy is also improved when a threshold changes in a direction which classifies pixels less into a target class. Thus, these accuracies are not suitable to evaluate a threshold because it is possible that those are improved by an unfair threshold.

Accordingly, we use a new accuracy to evaluate a threshold to estimate the quantities of class populations. We call the new accuracy a “counting accuracy” in this paper and define it as

$$C_i = \frac{n_{i+}}{N_i} \quad (8)$$

The counting accuracy is a ratio between a quantity classified into class i and a correct quantity of class i . It directly compares a quantity classified into class i and a correct quantity of class i . So the counting accuracy can evaluate the result of classification directly and can evaluate also the threshold indirectly, when our purpose of classification is to estimate the quantities of classified populations.

3. FEATURE

Theory of the proposed method was presented in the second chapter. However, can the expected result be taken by the proposed method? A validation of the effects and the works using

a data set is needed. To confirm the feature of the suggested method, comparison analysis between the results of the proposed method and existing methods are conducted. At first, ten sample input images are prepared. Every sample images have two classes and consist of 1,000,000 pixels. Each class goes along gaussian distribution. Two examples of the probability density functions are shown in Figure 2. Then number of pixels N_i , average μ_i and standard deviation σ_i for each class are shown in Table 2, where i denotes class number. Each image has a different number of pixels and a different standard deviation for each class. The results in case that there are various distributions of each class can be confirmed by the analysis of using these sample images.

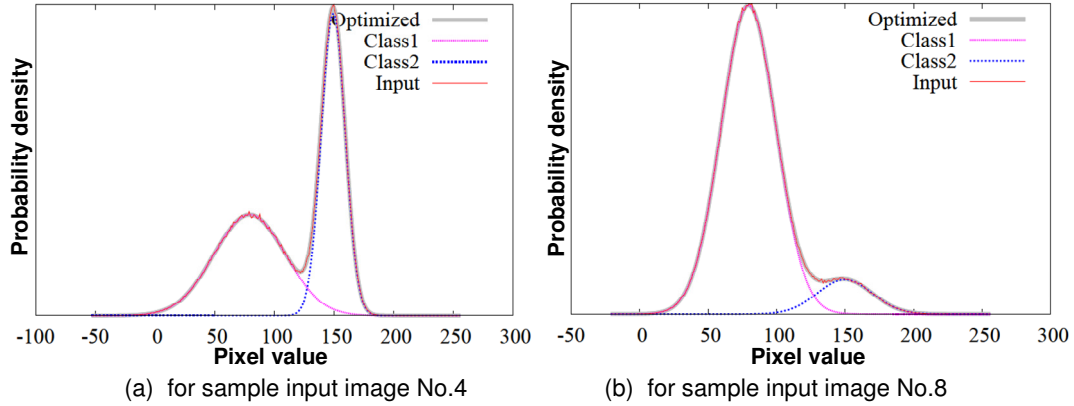


FIGURE 2: Example of the probability density function for each sample input image

TABLE 2: Then number of pixels N_i , average μ_i and standard deviation σ_i for each class

Sample input image	N_1	μ_1	σ_1	N_2	μ_2	σ_2
No.1	500,000	80	10	500,000	150	10
No.2	500,000	80	10	500,000	150	30
No.3	500,000	80	20	500,000	150	20
No.4	500,000	80	30	500,000	150	10
No.5	500,000	80	30	500,000	150	30
No.6	900,000	80	10	100,000	150	10
No.7	900,000	80	10	100,000	150	30
No.8	900,000	80	20	100,000	150	20
No.9	900,000	80	30	100,000	150	10
No.10	900,000	80	30	100,000	150	30

Selections of three thresholds using three methods are conducted respectively. One method is the proposed method while the other two methods are the Otsu's thresholding (hereinafter referred to as the Otsu thresholding) and the minimum error thresholding by Kittler and Illingworth's (hereinafter referred to as the Kitter thresholding). In case of Otsu thresholding, a threshold which makes $\eta = \sigma_B / \sigma_W$ maximum is selected by the downhill simplex method [26]. Where σ_B is intra-class variance and σ_W is inter-class variance. On the other hand, in case of the Kitlller thresholding, a threshold which makes an evaluation function J minimum is selected by the downhill simplex method. In the case of the proposed method, we optimized some parameters of a mixed gaussian distribution to match a probability density function of input image using the multivariate downhill simplex method. Then, we got a threshold which makes the criterion function

$\epsilon(k) = |e_1(k) - e_2(k)|$ minimum from some parameters of the mixed gaussian distribution using the downhill simplex method [26].

In the result, when numbers of pixels and standard deviations of two classes were equal (for sample image No.1, No.3 and No.5), each of the three thresholding methods selected same thresholds.

For each sample input image, we classified a pixel less than or equal to a threshold into class 1. In reverse, we classified a pixel bigger than a threshold into class 2. Then some classified images were created.

To evaluate the result of classifications, we compared the classified images with the correct classification results which we made first. Then, we made a confusion matrix which is shown in Table 1 from each result of evaluations. All elements of the confusion matrices for all evaluations are shown in Table 3. At the end, we calculated a overall accuracy O, a producer's accuracy P, a user's accuracy U and a counting accuracy C from the elements of the confusion matrices for each classifications. The results are shown in Table 4.

For sample input image No.1 and No.6 of which two classes were separated clearly, any accuracy of all methods was just about 100%. For sample input images of which the number of pixels and the standard deviations of the two classes were equal, the accuracies of each method did not differ clearly. However, for sample image No.2 and No.4 of which the standard deviations between the two classes were different, the most accurate overall accuracies were obtained by the Kittler thresholding. And the most exact counting accuracies were obtained by the proposed method. Furthermore, the Otsu method and the Kittler method make a big difference between a user's accuracy and a producer's accuracy. By contrast, the proposed method made a user's accuracy and a producer's accuracy approximate each other. Also for sample input images from No.6 to No.10, the most accurate counting accuracies were obtained by the proposed method being compared with other methods. Sample image No. 10 is convex shape. That means it is not biphasic distribution. However the proposed method can classify sample image No.10 with high accuracy. And the proposed method made the least difference between a user's accuracy and a producer's accuracy.

TABLE 3: Evaluated elements of confusion matrices

Sample image	Method	n_{11}	n_{12}	N_{1+}	N_1	n_{21}	n_{22}	n_{2+}	N_2
No.1	Otsu	499,886	102	499,988	500,000	114	499,898	500,012	500,000
	Kittler	499,888	106	499,994	500,000	112	499,894	500,006	500,000
	proposed	499,887	102	499,989	500,000	113	499,898	500,011	500,000
No.2	Otsu	414,754	6	414,760	500,000	85,246	499,994	585,240	500,000
	Kittler	466,625	3,144	469,769	500,000	33,375	496,856	530,231	500,000
	proposed	479,767	19,959	499,726	500,000	20,233	480,041	500,274	500,000
No.3	Otsu	479,842	19,984	499,826	500,000	20,158	480,016	500,174	500,000
	Kittler	479,904	20,051	499,955	500,000	20,096	479,949	500,045	500,000
	proposed	479,904	20,051	499,955	500,000	20,096	479,949	500,045	500,000
No.4	Otsu	499,995	84,938	584,933	500,000	5	415,062	415,067	500,000
	Kittler	496,668	32,943	529,611	500,000	3,332	467,057	470,389	500,000
	proposed	479,879	20,076	499,955	500,000	20,121	479,924	500,045	500,000
No.5	Otsu	439,178	60,812	499,990	500,000	60,822	439,188	500,010	500,000
	Kittler	438,272	59,885	498,157	500,000	61,728	440,115	501,843	500,000
	proposed	436,012	57,771	493,783	500,000	63,988	442,229	506,217	500,000
No.6	Otsu	99,974	238	100,212	100,000	26	899,762	899,788	900,000
	Kittler	99,922	64	99,986	100,000	78	899,936	900,014	900,000
	proposed	99,924	73	99,997	100,000	76	899,927	900,003	900,000
No.7	Otsu	84,797	36	84,833	100,000	15,203	899,964	915,167	900,000
	Kittler	90,152	718	90,870	100,000	9,848	899,282	909,130	900,000

	proposed	93,617	6,303	99,920	100,000	6,383	893,697	900,080	900,000
No.8	Otsu	99,059	117,060	216,119	100,000	941	782,940	783,881	900,000
	Kittler	80,660	3,773	84,433	100,000	19,340	896,227	915,567	900,000
	proposed	89,054	10,398	99,452	100,000	10,946	889,602	900,548	900,000
No.9	Otsu	100,000	302,704	402,704	100,000	0	597,296	597,296	900,000
	Kittler	99,977	109,844	209,821	100,000	23	790,156	790,179	900,000
	proposed	81,186	18,659	99,845	100,000	18,814	881,341	900,155	900,000
No.10	Otsu	97,213	297,742	394,955	100,000	2,787	602,258	605,045	900,000
	Kittler	87,928	109,509	197,437	100,000	12,072	790,491	802,563	900,000
	proposed	71,065	34,317	105,382	100,000	28,935	865,683	894,618	900,000

TABLE 4: Result of evaluation for each sample images (Overall accuracy, Producer's accuracy, User's accuracy and Counting accuracy for each class)

Sample image	Method	O	P ₁	U ₁	C ₁	P ₂	U ₂	C ₂
No.1	Otsu	100.0%	100.0%	100.0%	100.0%	100.0%	100.0%	100.0%
	Kittler	100.0%	100.0%	100.0%	100.0%	100.0%	100.0%	100.0%
	proposed	100.0%	100.0%	100.0%	100.0%	100.0%	100.0%	100.0%
No.2	Otsu	91.5%	83.0%	100.0%	83.0%	100.0%	85.4%	117.1%
	Kittler	96.4%	93.3%	99.3%	94.0%	99.4%	93.7%	106.1%
	proposed	96.0%	96.0%	96.0%	100.0%	96.0%	96.0%	100.1%
No.3	Otsu	96.0%	96.0%	96.0%	100.0%	96.0%	96.0%	100.0%
	Kittler	96.0%	96.0%	96.0%	100.0%	96.0%	96.0%	100.0%
	proposed	96.0%	96.0%	96.0%	100.0%	96.0%	96.0%	100.0%
No.4	Otsu	91.5%	100.0%	85.5%	117.0%	83.0%	100.0%	83.0%
	Kittler	96.4%	99.3%	93.8%	105.9%	93.4%	99.3%	94.1%
	proposed	96.0%	96.0%	96.0%	100.0%	96.0%	96.0%	100.0%
No.5	Otsu	87.8%	87.8%	87.8%	100.0%	87.8%	87.8%	100.0%
	Kittler	87.8%	87.7%	88.0%	99.6%	88.0%	87.7%	100.4%
	proposed	87.8%	87.2%	88.3%	98.8%	88.5%	87.4%	101.2%
No.6	Otsu	100.0%	100.0%	99.8%	100.2%	100.0%	100.0%	100.0%
	Kittler	100.0%	99.9%	99.9%	100.0%	100.0%	100.0%	100.0%
	proposed	100.0%	99.9%	99.9%	100.0%	100.0%	100.0%	100.0%
No.7	Otsu	98.5%	84.8%	100.0%	84.8%	100.0%	98.3%	101.7%
	Kittler	98.9%	90.2%	99.2%	90.9%	99.9%	98.9%	101.0%
	proposed	98.7%	93.6%	93.7%	99.9%	99.3%	99.3%	100.0%
No.8	Otsu	88.2%	99.1%	45.8%	216.1%	87.0%	99.9%	87.1%
	Kittler	97.7%	80.7%	95.5%	84.4%	99.6%	97.9%	101.7%
	proposed	97.9%	89.1%	89.5%	99.5%	98.8%	98.8%	100.1%
No.9	Otsu	69.7%	100.0%	24.8%	402.7%	66.4%	100.0%	66.4%
	Kittler	89.0%	100.0%	47.7%	209.8%	87.8%	100.0%	87.8%
	proposed	96.3%	81.2%	81.3%	99.9%	97.9%	97.9%	100.0%
No.10	Otsu	70.0%	97.2%	24.6%	395.0%	66.9%	99.5%	67.2%
	Kittler	87.8%	87.9%	44.5%	197.4%	87.8%	98.5%	89.2%
	proposed	93.7%	71.1%	67.4%	105.4%	96.2%	96.8%	99.4%

It should be noted that the Otsu method and the Kittler method make a big difference between a user's accuracy and a producer's accuracy, because these methods make a big difference between the number of classified pixels n_{i+} and the number of correct classification pixel N_i too. On the other hand, the proposed method decreases the difference between a user's accuracy and a producer's accuracy, because the method makes the number of classified pixels n_{i+} and the number of correct classification pixel N_i approximate each other. Accordingly, the proposed method can select a threshold to improve the counting accuracy C. In other words, the proposed method can estimate the number of pixels of a class with more precision than other methods.

4. RANGE OF APPLICATION

The proposed method selects a threshold by statistical algorithm. Thus, a sufficient number of input data are required in order to stabilize a result. Verifying analysis of a sufficient quantity of input data to stabilize a threshold and a classification under the assumption of estimating a planting area of paddy using a SAR data (RADARSAT-2, Ultra-Fine, 2009/6/6) from a satellite is conducted.

At first, inspection of a distribution of backscattering coefficients of SAR data for each field is implemented. Then it becomes clear that the distribution is similar to a mixed gaussian distribution (refer to Figure 3) . Some input data sets which have 10 to 10,000,000 sample data and the same distribution are prepared. At the Time, a class of the sample data belongs was defined in order to evaluate accuracies after classifications.

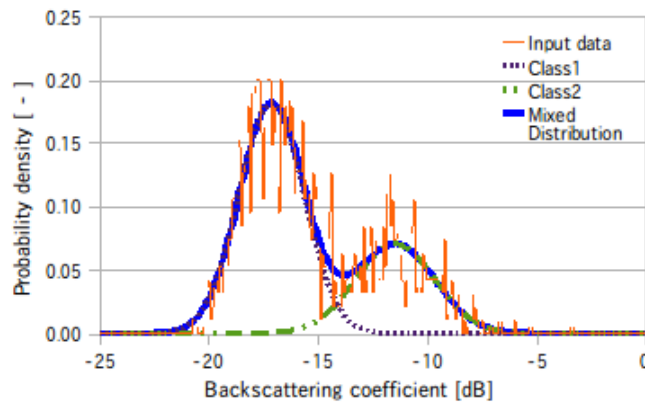


FIGURE 3: A result of optimization of a mixed distribution which used RADARSAT-2 data

As a result of validation of the stable number of input samples, stable thresholds were not obtained when we used less than 1000 samples with this distribution data. In contrast, stable thresholds were obtained using more than 1000 samples by any threshold method (refer to Figure 4).

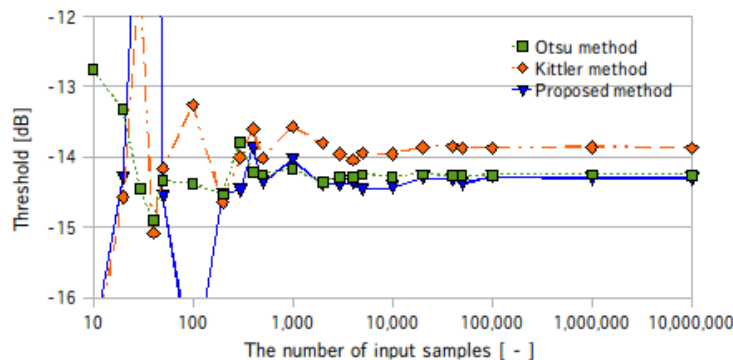


FIGURE 4: Variation in a threshold when the number of input samples was changed.

Furthermore, as a result of evaluating accuracies of classifications, accuracies of each method were reversed at each data set when we used less than 10,000 samples for evaluation. In other

hand, stable accuracies were obtained when we used more than 10,000 samples. This means that 10,000 samples are required at least (refer to Figure 5 and Figure 6).

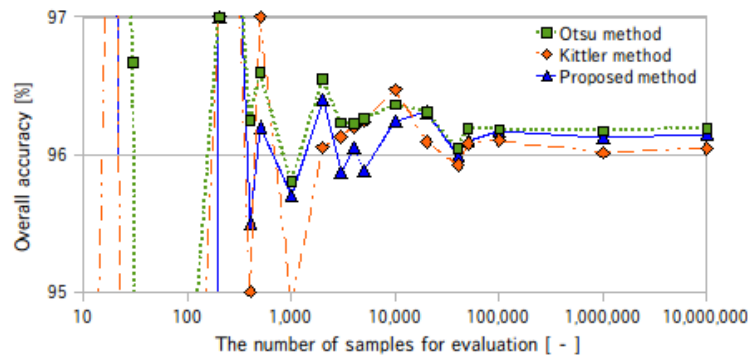


FIGURE 5: Variation in a overall accuracy when the number of input samples was changed.

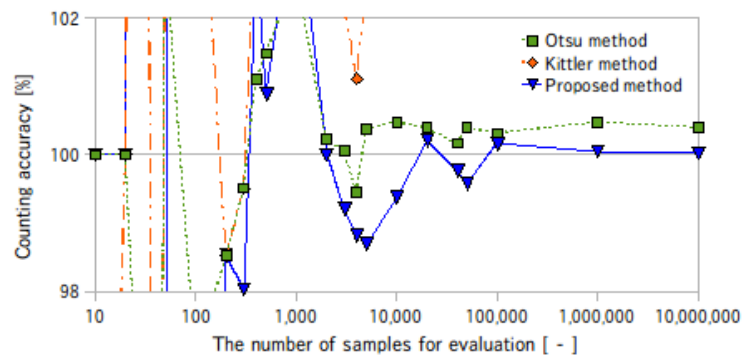


FIGURE 6: Variation in a counting accuracy when the number of input samples was changed.

Accordingly, distributions with at least 1,000 samples are required in order to obtain a stable threshold. And at least 10,000 samples are required in order to compare the accuracies of each thresholding method.

5. CONCLUSION

In conclusion, the method we proposed can select a threshold which equalizes two amounts of incorrect classifications of each class. This method has a unique objective which is to select a threshold to estimate the total number of data (pixels) of each classified population. Furthermore by comparing the proposed method with the existing methods, we showed the proposed method has the following advantages.

- A higher counting accuracy can be obtained than with the existing methods.
- The method can equalize a user's accuracy and a producer's accuracy more than the other methods.
- The proposed method is valid even if there are biases of amounts and deviations in each class.
- The proposed method is valid even if input data do not have a biphasic distribution.

The distribution characteristics of input data must be known when the proposed method is utilized. In addition, the application of proposed method has the following characteristics:

- The proposed method can be used not only for an image data but also for a numerical data.
- At least 1,000 samples are required in order to obtain a stable threshold.
- At least 10,000 samples are required in order to compare with the accuracies of some thresholding methods.

For actual applications, sometimes the number of input data and true data for evaluation are not sufficiency. In this case, it is difficult to apply the proposed method into the analysis. Furthermore, it is also difficult to use an input data having a unknown distribution as input class. This is because an assuming or a knowing a distributed shape is needed for the proposed method.

It should be noted that the result is an example for estimating a planting area of paddy using some specific data. We showed some characteristics and ranges of application of the proposed method. The method has some advantages for thresholding and classification. However, the most specified characteristic of the proposed method is its objective. A purpose of the existing methods is to decrease errors of a classification. On the other hand, the purpose of the proposed method is to estimate quantities, data volumes, of classes through a classification analysis. Of course, classical statistic method could estimate quantity of a class. But it cannot classify sample data. The proposed method can coordinate a result of a classification and a result of quantity estimation. The proposed method is definitely useful when both classification and quantity estimation of a class are required.

Almost all data have some noise. So, validations of resistance to some noises will be conducted in the future. After an adaptive limits are known, solutions which can be applied the proposed method will be findable. Application of the proposed method to various field analyses would be a major topic in next step.

6. ACKNOWLEDGEMENT

I am deeply grateful to Imageone Co. Ltd. for providing RADARSAT-2 data to us. Special thanks also Mr. Toshio Azuma whose comments and suggestions were innumerably valuable.

7. REFERENCES

- [1] P. K. Sahoo, S. Soltani, and A. K. C. Wong, (1988), "*A Survey of Thresholding Techniques*", Computer Vision Graphics and Image Processing, Vol. 41, pp. 233-260.
- [2] W. Doyle, (1962), "*Operation useful for similarity-invariant pattern recognition*", J. Assoc. Comput.er, Vol. 9, pp. 259-267.
- [3] J. M. S. Prewitt and M. L. Mendelsohn, (1983), "*The analysis of cell images*", in Ann. New York Acad. Sci. Vol128, pp 1035-1053, New York Acad. Sci., New York, 1966.
- [4] T. Pun, (1980), "*A new method for gray-level picture thresholding using the entropy of the histogram*", Signal Process. Vol. 2, pp. 223-237.
- [5] J. N. Kapur, P. K. Sahoo, and A. K. C. Wong, (1985), "*A new method for gray-level picture thresholding using the entropy of the histogram*", Computer. Vision Graphics Image Process. Vol. 29, pp. 273-285.
- [6] G. Johannsen and J. Bille, (1982), "*A threshold selection method using information measures*", in Proceedings, 6th Znt. Conf. Pattern Recognition, Munich, Germany, pp. 140-143.
- [7] W. Tsai, (1985), "*Moment-preserving thresholding: A new approach*", Computer Vision Graphics Image Process. Vol. 29, pp. 377-393.
- [8] D. Mason, I. J. Lauder, D. Rutoritz, and G. Spowart, (1975), "*Measurement of C-Bands in human chromosomes*", Computer. Biol. Med. Vol. 5, pp. 179-201.

- [9] N. Ahuja and A. Rosenfeld, (1978), "A note on the use of second-order gray-level statistics for threshold selection", IEEE Trans. Systems Man Cybernet. SMC-8, pp. 895-899.
- [10] R. L. Kirby and A. Rosenfeld, (1979), "A note on the use of (gray level, local average gray level) space as an aid in thresholding selection", IEEE Trans. Systems Man Cybernet. SMC-9, pp. 860-864.
- [11] F. Deravi and S. K. Pal, (1983), "Gray level thresholding using second-order statistics", Pattern Recognit. Zett. Vol. 1, pp. 417-422.
- [12] R. Southwell, (1940), "Relaxation Methods in Engineering Science, A Treatise on Approximate Computation", Oxford Univ. Press, London.
- [13] S. Boukharouba, J. M. Rebordao, and P. L. Wendel, (1985), "An amplitude segmentation method based on the distribution function of an image", Computer Vision Graphics Image Process. Vol. 29, pp. 47-59.
- [14] S. Wang and R. M. Haralick, (1984), "Automatic multithreshold selection", Computer Vision Graphics Image Process. Vol. 25, pp. 46-67.
- [15] R. Kohler, (1981), "A segmentation system based on thresholding", Computer Graphics Image Process. Vol. 15, pp. 319-338.
- [16] N. Otsu. (1980, App.). "An Automatic Threshold Selection Method Based on Discriminant and Least Squares Criteria." IEICE TRANSACTIONS on Fundamentals of Electronics. Vol. J63-D(4), pp. 349-356.
- [17] N. Otsu. (1979, Jan.). "A Thresholding Selection Method from Gray-Level Histograms." IEEE Transaction on Systems, Man, And Cybernetics, Vol. SMC-9(1), pp. 62-66.
- [18] J. Kittler and J. Illingworth. (1986). "Minimum Error Thresholding." Pattern Recognition, Vol. 19(1), pp. 41-47.
- [19] J. Kittler. (2004). "Fast branch and bound algorithms for optimal feature selection." IEEE Transactions on Pattern Analysis and Machine Intelligence, Vol. 26(7), pp. 900-912.
- [20] I. Sekita, T. Kurita, N. Otsu and N. N. Abdelmalek. (1995, Dec.). "Thresholding Methods Considering the Quantization Error of an Image." IEICE TRANSACTIONS on Fundamentals of Electronics. Vol. J78-D-2(12), pp. 1806-1812.
- [21] T. Kurita, N. Otsu and N. Abdelmalek (1992, Oct.). "Maximum Likelihood Thresholding Based on Population Mixture Models." Pattern Recognition, Vol. 25(10), pp. 1231-1240.
- [22] M. Katoh, T. Tsushima and M. Kanno. (1999, Nov.). "Monitoring of Ishikari river model forest for sustainable forest management, Grasp and monitor of forest area using satellite data." Hoppou Ringyo. Vol. 51(11), pp. 271-274.
- [23] H. Takeuchi, T. Konishi, Y. Suga and Y. Oguro. (2000, Sep.). "Rice-Planted Area Estimation in Early Stage Using Space-Borne SAR Data." Journal of the Japan Society of Photogrammetry. Vol. 39(4), pp. 25-30.
- [24] W. Takeuchi, Y. Yasuoka. (2005, Jan.). "Mapping of fractional coverage of paddy fields over East Asia using MODIS data." Journal of the Japan Society of Photogrammetry. Vol. 43(6), pp. 20-33.
- [25] A. Sutaryanto, M. Kunitake, S. Sugio and C. Deguchi. (1995, May). "Calculation of Percent Imperviousness by using Satellite Data and Application to Runoff Analysis." Journal of the Agricultural Engineering Society Japan, Vol. 63(5), pp. 23-28.
- [26] K. Amaya. (2008, May). *Kougaku no tameno saitekika shuhou nyuumon [Introduction to optimization techniques for engineering]*. Tokyo: Suuri Kougakusha, 2008.
- [27] K. Arai and X. Liang. (2003, App.). "Method for Estimation of Refractive Index and Size Distribution of Aerosol Using Direct and Diffuse Solar Irradiance as well as Aureole by Means of a

Modified Simulated Annealing.” The Journal of the Remote Sensing Society of Japan. Vol. 23(1), pp. 11-20.

[28] G. M. Foody. “*Classification Accuracy Assessment.*” IEEE Geoscience and Remote Sensing Society Newsletter(2011, Jun.), pp 8-14, 2011.

INSTRUCTIONS TO CONTRIBUTORS

International Journal of Applied Sciences (IJAS) is publishing articles in all areas of applied sciences. IJAS seeks to promote and disseminate knowledge in the applied sciences, natural and social sciences industrial research materials science and technology, energy technology and society including impacts on the environment, climate, security, and economy, environmental sciences, physics of the games, creativity and new product development, professional ethics, hydrology and water resources, wind energy. IJAS is an academic peer reviewed on-line international journal of broad appeal aimed at fast publication of cutting edge multidisciplinary research articles reporting on original research across the fields of pure and applied sciences.

To build its International reputation, we are disseminating the publication information through Google Books, Google Scholar, Directory of Open Access Journals (DOAJ), Open J Gate, ScientificCommons, Docstoc and many more. Our International Editors are working on establishing ISI listing and a good impact factor for IJAS.

The initial efforts helped to shape the editorial policy and to sharpen the focus of the journal. Starting with Volume 4, 2013, IJAS will be appearing with more focused issues. Besides normal publications, IJAS intend to organized special issues on more focused topics. Each special issue will have a designated editor (editors) – either member of the editorial board or another recognized specialist in the respective field.

We are open to contributions, proposals for any topic as well as for editors and reviewers. We understand that it is through the effort of volunteers that CSC Journals continues to grow and flourish.

IJAS LIST OF TOPICS

The realm of International Journal of Applied Sciences (IJAS) extends, but not limited, to the following:

- Agricultura
- Audio
- Automotive Engineering
- Biological
- Bombs
- Building officials
- Chemical
- Combat Engineering
- Cryogenics
- Domestic Educational Technologies
- Energy
- Engineering geology
- Entertainment
- Environmental Engineering Science
- Environmental technology
- Fire Protection Engineering
- Fishing
- Food Technology
- Health Safety
- Industrial Technology
- Machinery
- Architectural
- Automotive
- Biochemical
- Biomedical
- Broadcast
- Ceramic
- Civil
- Construction
- Domestic appliances
- Domestic Technology
- Energy storage
- Enterprise
- Environmental
- Environmental Risk Assessment
- Financial Engineering
- Fisheries science
- Food
- Genetic
- Health Technologies
- Industry Business Informatics
- Manufacturing

- Marine Engineering
- Materials science and engineering
- Metallurgical
- Military Ammunition
- Military Technology and equipment
- Motor Vehicles
- Naval Engineering
- Nutrition
- Ontology
- Optics
- Pharmaceuticals
- Sanitary Engineering
- Textile
- Traffic
- Visual Technology
- Material Sciences
- Medical Technology
- Microtechnology
- Military Technology
- Mining
- Music
- Nuclear technology
- Ocean
- Optical
- Particle physics
- Safety Engineering
- Space Technology
- Tissue
- Transport
- Zoography

CALL FOR PAPERS

Volume: 4 - Issue: 1

i. Paper Submission: February 28, 2013

ii. Author Notification: May 31, 2013

iii. Issue Publication: June 2013

CONTACT INFORMATION

Computer Science Journals Sdn Bhd

B-5-8 Plaza Mont Kiara, Mont Kiara
50480, Kuala Lumpur, MALAYSIA

Phone: 006 03 6207 1607
006 03 2782 6991

Fax: 006 03 6207 1697

Email: cscpress@cscjournals.org

CSC PUBLISHERS © 2012
COMPUTER SCIENCE JOURNALS SDN BHD
M-3-19, PLAZA DAMAS
SRI HARTAMAS
50480, KUALA LUMPUR
MALAYSIA

PHONE: 006 03 6207 1607
006 03 2782 6991

FAX: 006 03 6207 1697
EMAIL: cscpress@cscjournals.org